TITLE PAGE

Quantitative PET and histology of brain biopsy reveal lack of selective Pittsburgh compound-B binding to intracerebral amyloidoma

Colin Groot, MSc[a,b,*,†], Nelleke Tolboom, MD, PhD[b,†], Milos D. Ikonomovic, MD[d,e,f], Adriaan A. Lammertsma, PhD[b], Baayla D.C. Boon[a,c], Frederik Barkhof, MD, PhD[b,g], Philip Scheltens, MD, PhD[1], William E. Klunk, MD, PhD[d,e], Annemieke J.M. Rozemuller, MD, PhD[c], Rik Ossenkoppele, PhD[a,b] & Bart N.M. van Berckel, MD, PhD[b]

Departments of Neurology & Alzheimer Center[a], Radiology & Nuclear Medicine[b] and Pathology[c], VU University Medical Center, Amsterdam, The Netherlands

Department of Neurology[d] and Psychiatry[e], University of Pittsburgh School of Medicine, Pittsburgh, Pennsylvania, USA; Geriatric Research Education and Clinical Center[f], Veterans Administration Pittsburgh Healthcare System, Pittsburgh, Pennsylvania, USA; Institutes of Neurology and Healthcare Engineering[g], UCL, London, UK

[*] **Correspondence to first author**: Colin Groot, VU University Medical Center, de Boelelaan 1117, Amsterdam, E-mail: c.groot3@vumc.nl, tel: 0031204445240, fax: 0031204448529.

[†] These authors contributed equally

Running title: PiB-PET and histology in amyloidoma

ABSTRACT

This case study examines selective Pittsburgh compound-B (PiB) binding to an intracerebral light-chain amyloidoma using a 90-minute dynamic [^{11}C]PiB-PET scan and brain biopsy tissue. Parametric non-displaceable binding potential (BP$_{ND}$) images showed negligible specific binding in the amyloidoma, while relative tracer delivery (R$_I$) was adequate. Histology of the tissue revealed strong colouring with congo-red, thioflavin-S, and X-34, indicating presence of amyloid. However, immunological staining with 6F/3D revealed absence of amyloid-β and histofluorescence of 6-CN-PiB, a highly fluorescent derivative of PiB, was negligible. These results suggest that PiB does not detect the atypical amyloid pathology associated with an intracerebral light-chain amyloidoma.

INTRODUCTION

The development of positron emission tomography (PET) amyloid ligands such as [^{11}C]Pittsburgh compound-B (PiB) [1], have provided a non-invasive tool to assess amyloid-β (Aβ) pathology *in vivo*. PiB has been shown to bind strongly to fibrillary Aβ$_{40-42}$ [2,3], and elevated binding of [^{11}C]PiB is consistently observed in patients with sporadic Alzheimer's disease (AD) [4], even in very early stages of the disease.[5] However, several studies reported undetectable levels of [^{11}C]PiB PET retention in subjects with histologically detectable, albeit non abundant, Aβ pathology at time of autopsy or biopsy.[6-8] In addition, there are exceptional cases where [^{11}C]PiB retention was low in patients clinically diagnosed with AD [9-11], even in the presence of heavy cortical Aβ deposition in post-mortem tissue.[10] Furthermore, in contrast to findings in APP duplication, Swedish APP mutation and presenilin-1/2 mutation carriers who all show levels of [^{11}C]PiB retention typical of late-onset AD [12, 13], patients with the "Arctic" APP mutation display very low [^{11}C]PiB retention, while cerebrospinal fluid levels of Aβ$_{1-42}$ indicate presence of amyloid pathology.[14] An explanation for this discrepancy is offered by histological examination in "Arctic" APP carriers which revealed that amyloid depositions in these patients are mainly characterized by non-fibrillary amyloid pathology, such as protofibrils and oligomers.[15.16] *In vitro* and animal studies have shown that, at nanomolar concentrations administered to the living human brain, [^{11}C]PiB does not bind equally to all isoforms [2,17-19] and conformations [3,20] of amyloid equally.

Here we present a case of a 52 year-old woman with an intracerebral light-chain amyloidoma, a form of solitary localised, tumoral amyloidosis.[21-23] The diagnosis of intracerebral amyloidoma is made on the basis of histological examination of biopsy material, which is obtained through an invasive procedure. We

3

examined whether the atypical form of amyloid pathology found in intracerebral amyloidoma can also be visualized *in vivo* with [11C]PiB-PET imaging, by quantitatively assessing [11C]PiB binding in combination with histology from a brain biopsy performed during life.

MATERIALS AND METHODS

Case description

The 52 year-old patient was referred to the hospital because of an epileptic seizure. Her past medical history was uneventful. However, in the period leading up to the epileptic seizure, a remarkable change in personality was observed with a lack of initiative. Magnetic resonance imaging (MRI) revealed an intracranial solid neoplasm within the white matter of the right frontal lobe with both high and low intensities on T1 (Figure 1A) and FLAIR (Figure 1B). Administration of gadolinium showed a patchy enhancement of the lesion and spectroscopic examination revealed low N-acetyl aspartate and high choline levels, without lipids or lactate. All observations considered, the most probable diagnosis was an intracerebral amyloidoma.[21-23] Brain biopsy was performed to confirm this suspicion, which indeed revealed histological evidence for light-chain amyloidosis (not shown).[24] [11C]PiB and [18F]FDG-PET scans were performed two years after the diagnosis was made, and the remains of the brain biopsy were examined with additional histological stains. All procedures performed were in accordance with the ethical standards of the institutional research committee and with the 1964 Helsinki declaration and its later amendments. Informed consent was obtained from all individual participants included in the study.

PET imaging

A 90-minute dynamic $[^{11}C]$PiB-PET scan protocol was performed using an ECAT EXACT HR+ scanner (CTI/Siemens, Knoxville, TN, USA). PET sinograms were corrected for dead time, tissue attenuation, decay, scatter, and randoms. Next, data was reconstructed using a standard filtered back projection algorithm and a Hanning filter with a cut-off at 0.5 times the Nyquist frequency. A matrix size of 256x256x63 was used, resulting in a voxel size of 1.2x1.2x2.4 mm and spatial resolution of approximately 7 mm full width at half-maximum at the center of the field of view. An MR image was aligned to the PET image using a mutual-information algorithm and PVE-lab, a software program that uses a probability map [25], was used to project PET data onto the structural MRI. PET data were analyzed using receptor parametric mapping with fixed efflux rate constant (RPM2) [26], generating parametric non-displaceable binding potential (BP_{nd}) and R_1 images using cerebellar gray matter as reference tissue. R_1 represents the relative tracer delivery to the target tissue and provides an indication of flow. Furthermore, a standardized uptake value ratio (SUVr, 60-90 minute) image was generated using cerebellar gray matter as reference. Detailed information on scanning protocol and data analysis procedures are described elsewhere.[26]

We visually assessed the amyloidoma on $[^{11}C]$PiB-R_1, BP_{nd} and SUVr images. Furthermore, $[^{11}C]$PiB-R_1, BP_{nd} and SUVr values were also assessed quantitatively by manually delineating the amyloidoma on MRI and calculating these parameters within the amyloidoma using an volume-of-interest (VOI) delineation tool. This VOI tool is built in-house and is used to manually draw VOI on MRI or PET images. The tool provides with a binary image of VOI that can be superimposed onto the PET scan to extract the time activity curve i.e the average activity in the VOI over time.

R$_1$, BP$_{nd}$ and SUVr values within the volume of the amyloidoma were compared with values in a contralateral VOI, which matched the size and anatomical location of the amyloidoma (Figure 2). Finally, for the [^{18}F]FDG PET scan we generated a SUVr image for the interval between 45-60 minute using cerebellar gray matter as the reference region.[26]

Histology

The tissue of the amyloidoma acquired by brain biopsy during life was examined using staining for congo-red and thioflavin-S, and immunologic staining for amyloid-β (using the monoclonal antibody 6F/3D [27]). Tissue from the amyloidoma was then additionally assessed using histofluorescence of 6-CN-PiB [28] (a highly fluorescent derivative of PiB), and X-34 [29] (a highly fluorescent derivative of congo red). As a reference, histofluorescence of 6-CN-PiB and X-34 was also assessed in frontal cortical tissue sections from an end-stage Alzheimer's disease (AD) patient as a "positive control".

RESULTS

PET imaging

[^{18}F]FDG revealed a large hypometabolic region in the right frontal lobe extending beyond the location of the amyloidoma (Figure 1C). [^{11}C]PiB-PET showed low binding in cortical areas with relatively high uptake in the subcortical white matter (Figure 1D,E), similar to patterns observed in most healthy controls.[1] At the location of the amyloidoma, within the white matter, [^{11}C]PiB binding was low, as indicated by both BP$_{ND}$ (Figure 1D) and SUVr (Figure 1E) images. BP$_{ND}$ within the volume of the amyloidoma (8.60 mL) was 0.24, whilst BP$_{ND}$ within the volume of the contralateral

VOI (6.57 mL) was 0.46. Corresponding SUVr values for amyloidoma and contralateral VOI were 1.33 and 1.44, respectively. Furthermore, the R_1 image showed that tracer delivery to the amyloidoma (Figure 1F), was only slightly lower than to the contralateral VOI (0.44 and 0.56, respectively).

Histology

The brain biopsy tissue was clearly positive with congo-red (Figure 3A) and thioflavin-S staining (Figure 3B), indicating presence of amyloid. However, immunological staining with 6F/3D revealed that there was no amyloid-β present in the amyloidoma tissue (Figure 3C). Additional histological examinations revealed a prominent staining of amyloid with X-34, similar as in the AD "positive control" (Figure 3D,E), again indicating the presence of amyloid. However, 6-CN-PiB was at background levels compared with the robust plaque staining in the same region of the AD case (Figure 3F,G).

DISCUSSION

Our results indicate that [^{11}C]PiB does not bind cerebral amyloid pathology associated with a light-chain intracerebral amyloidoma. Quantitative analysis revealed that [^{11}C]PiB binding was negligible, despite tracer being delivered to the tissue. Furthermore, histological examination of brain biopsy tissue revealed a convincing explanation for the lack of [^{11}C]PiB binding, as the strong colouring with congo-red, thioflavin-S and X-34 were suggestive of presence of amyloid, but the lack of 6F/3D staining indicated that there was no fibrillary amyloid-β pathology present. Furthermore, in keeping with the [^{11}C]PiB-PET findings we observed no histofluoresence of 6-CN-PiB in the amyloidoma tissue. These results highlight that

7

PiB selectively binds to fibrillar Aβ pathology [2,3], and does not detect the atypical amyloid pathology found in this case of intracerebral amyloidoma.

To date, only one other study assessing accordance between *in vivo* amyloid imaging and histology in intracerebral amyloidoma has been published.[30] Contrary to our findings, PET imaging with [^{18}F]Florbetapir (a different amyloid-β tracer) revealed slightly increased uptake in the region of the amyloidoma and histology showed weak staining for amyloid-β. One explanation for this discrepancy could be the heterogeneity between subjects (e.g. the absence or presence of fibrillary amyloid-β in the amyloidoma) as previous literature has described cases of intracerebral amyloidoma with histological evidence for amyloid-β (see [23] for a review). More likely, however, are factors associated with the pharmacokinetics of the different tracers. [^{18}F] amyloid imaging ligands tend to show higher nonspecific uptake in white matter [31], which may, due to the location of the amyloidoma (within the white matter), have convoluted interpretation of results. In addition, two studies [32,33] have reported PiB detection of systemic light-chain amyloidosis. One study assessed *in vivo* [11C]PiB-PET binding in the heart [32] and the other assessed *in vitro* [^{3}H]PiB binding in the liver and spleen [33]. However, the affinity of [^{3}H]PiB for systemic amyloid was 448 ± 185nM in these systemic tissues; compared to 3.84 ± 0.04nM in AD brain [33]. Such low-affinity binding would not be expected to be detectable with *in vivo* brain PET.

Strengths of the present study include the implementation of a dynamic PET scan, which enabled us to assess tracer delivery (R_1) and [^{11}C]PiB binding in a quantitative manner.[26] Furthermore, the study is unique in combining dynamic [^{11}C]PiB-PET with histological examination of biopsy material. Some limitations of the present study also need to be taken into account. Localized amyloidosis,

characteristic of the amyloidoma, rarely affects the brain. Consequently, literature on this topic is sparse, with only around 30 cases having been described.[21-23, 30] This paucity of available literature, in combination with the heterogeneity in clinical and radiological presentations across cases, prevents us from making any conclusions about intracerebral amyloidoma in general.

Taken together, our results highlight the selective binding of [^{11}C]PiB to fibrillary Aβ and indicate that [^{11}C]PiB does not bind to amyloid pathology associated with light-chain intracerebral amyloidoma.

REFERENCES

1   Klunk WE, Engler H, Nordberg A, Wang Y, Blomqvist G, Holt DP, Bergström M, Savitcheva I, Huang GF, Estrada S, Ausén B, Debnath ML, Barletta J, Price JC, Sandell J, Lopresti BJ, Wall A, Koivisto P, Antoni G, Mathis CA, Långström B(2004) Imaging brain amyloid in Alzheimer's disease with Pittsburgh Compound-B. *Ann Neurol* 55(30), 306-319.

2   Klunk WE, Lopresti BJ, Ikonomovic MD, Lefterov IM, Koldamova RP, Abrahamson EE, Debnath ML, Holt DP, Huang GF, Shao L, DeKosky ST, Price JC, Mathis CA (2005) Binding of the positron emission tomography tracer Pittsburgh compound-B reflects the amount of amyloid-beta in Alzheimer's disease brain but not in transgenic mouse brain. *J Neurosci* 25(46), 10598-10606.

3   Ikonomovic MD, Klunk WE, Abrahamson EE, Mathis CA, Price JC, Tsopelas ND, Lopresti BJ, Ziolko S, Bi W, Paljug WR, Debnath ML, Hope CE, Isanski BA, Hamilton RL, DeKosky ST (2008) Post-mortem correlates of in vivo PiB-PET amyloid imaging in a typical case of Alzheimer's disease. *Brain* 131(6), 1630-1645.

4   Nordberg A. Amyloid plaque imaging in vivo: current achievement and future prospects (2008) *Eur J Nucl Med Mol Imaging* 35(1), 46-50.

5   Pike KE, Savage G, Villemagne VL, Ng S, Moss SA, Maruff P, Mathis CA, Klunk WE, Masters CL, Rowe CC (2007) Beta-amyloid imaging and memory in non-demented individuals: evidence for preclinical Alzheimer's disease. *Brain* 130(11), 2837-2844.

6   Cairns NJ, Ikonomovic MD, Benzinger T, Storandt M, Fagan AM, Shah AR, Reinwald LT, Carter D, Felton A, Holtzman DM, Mintun MA, Klunk WE, Morris JC (2009) Absence of Pittsburgh compound B detection of cerebral amyloid beta in a

patient with clinical, cognitive, and cerebrospinal fluid markers of Alzheimer disease: a case report. *Arch Neurol* 66(12), 1557-1562.

7   Ikonomovic MD, Abrahamson EE, Price JC, Hamilton RL, Mathis CA, Paljug WR, Debnath ML, Cohen AD, Mizukami K, DeKosky ST, Lopez OL, Klunk WE (2012) Early AD pathology in a [C-11]PiB-negative case: a PiB-amyloid imaging, biochemical, and immunohistochemical study. *Acta Neuropathol* 123(3), 433-447.

8   Leinonen V, Alafuzoff I, Aalto S, Suotunen T, Savolainen S, Någren K, Tapiola T, Pirttilä T, Rinne J, Jääskeläinen JE, Soininen H, Rinne JO (2008) Assessment of beta-amyloid in a frontal cortical brain biopsy specimen and by positron emission tomography with carbon 11-labeled Pittsburgh Compound B. *Arch Neurol* 65(10), 1304-1309.

9   Li Y, Rinne JO, Mosconi L, Pirraglia E, Rusinek H, DeSanti S, Kemppainen N, Någren K, Kim BC, Tsui W, de Leon MJ (2008) Regional analysis of FDG and PIB-PET images in normal aging, mild cognitive impairment, and Alzheimer's disease. *Eur J Nucl Med Mol Imaging* 35(12), 2169-2181.

10   Rosen RF, Ciliax BJ, Wingo TS, Gearing M, Dooyema J, Lah JJ, Ghiso JA, LeVine H 3rd, Walker LC (2010) Deficient high-affinity binding of Pittsburgh compound B in a case of Alzheimer's disease. *Acta Neuropathol* 119(2), 221-233.

11   Edison P, Archer HA, Hinz R, Hammers A, Pavese N, Tai YF, Hotton G, Cutler D, Fox N, Kennedy A, Rossor M, Brooks DJ (2007) Amyloid, hypometabolism, and cognition in Alzheimer disease: an [11C]PIB and [18F]FDG PET study. *Neurology* 68(7), 501-508.

12   Villemagne VL, Ataka S, Mizuno T, Brooks WS, Wada Y, Kondo M, Jones G, Watanabe Y, Mulligan R, Nakagawa M, Miki T, Shimada H, O'Keefe GJ, Masters

CL, Mori H, Rowe CC (2009) High striatal amyloid beta-peptide deposition across different autosomal Alzheimer disease mutation types. *Arch Neurol* 66(12), 1537-44.

13   Remes AM, Laru L, Tuominen H, Aalto S, Kemppainen N, Mononen H, Någren K, Parkkola R, Rinne JO (2008) Carbon 11-labeled pittsburgh compound B positron emission tomographic amyloid imaging in patients with APP locus duplication. *Arch Neurol* 65(4), 540-544.

14   Schöll M, Wall A, Thordardottir S, Ferreira D, Bogdanovic N, Långström B, Almkvist O, Graff C, Nordberg A (2012) Low PiB PET retention in presence of pathologic CSF biomarkers in Arctic APP mutation carriers. *Neurology* 79(3), 229-236.

15   Kalimo H, Lalowski M, Bogdanovic N, Philipson O, Bird TD, Nochlin D, Schellenberg GD, Brundin R, Olofsson T, Soliymani R, Baumann M, Wirths O, Bayer TA, Nilsson LN, Basun H, Lannfelt L, Ingelsson M (2013) The Arctic AβPP mutation leads to Alzheimer's disease pathology with highly variable topographic deposition of differentially truncated Aβ. *Acta Neuropathol Commun* 1, 60.

16   Nilsberth C, Westlind-Danielsson A, Eckman CB, Condron MM, Axelman K, Forsell C, Stenh C, Luthman J, Teplow DB, Younkin SG, Näslund J, Lannfelt L (2001) The 'Arctic' APP mutation (E693G) causes Alzheimer's disease by enhanced Abeta protofibril formation. *Nat Neurosci* 4(9):887-893.

17   Maeda J, Ji B, Irie T, Tomiyama T, Maruyama M, Okauchi T, Staufenbiel M, Iwata N, Ono M, Saido TC, Suzuki K, Mori H, Higuchi M, Suhara T (2007) Longitudinal, quantitative assessment of amyloid, neuroinflammation, and anti-amyloid treatment in a living mouse model of Alzheimer's disease enabled by positron emission tomography. *J Neurosci* 27(41), 10957-10968.

18   Rosen RF, Walker LC, Levine H 3rd (2009) PIB binding in aged primate brain: enrichment of high-affinity sites in humans with Alzheimer's disease. *Neurobiol Aging* 32(2), 223-234.

19   Svedberg MM, Hall H, Hellström-Lindahl E, Estrada S, Guan Z, Nordberg A, Långström B (2009) [(11)C]PIB-amyloid binding and levels of Abeta40 and Abeta42 in postmortem brain tissue from Alzheimer patients. *Neurochem Int* 54(5-6), 347-357.

20   Yamin G, Teplow DB (2017) Pittsburgh Compound-B (PiB) binds amyloid β-protein protofibrils. *J Neurochem* 140(2), 210-215.

21   Spaar FW, Goebel HH, Volles E, Wickboldt J (1981) Tumor-like amyloid formation(amyloidoma) in the brain. *J Neurol* 224(3), 171-182.

22   Foreid H, Barroso C, Evangelista T, Campos A, Pimentel J (2010) Intracerebral amyloidoma: case report and review of the literature. *Clin Neuropathol* 29(4), 217-222.

23   Miller-Thomas MM, Sipe AL, Benzinger TL, McConathy J, Connolly S, Schwetye KE (2016) Multimodality review of amyloid-related diseases of the central nervous system. *Radiographics* 36(4), 1147-1163.

24   Laeng RH, Altermatt HJ, Scheithauer BW, Zimmermann DR (1998) Amyloidomas of the nervous system: a monoclonal B-cell disorder with monotypic amyloid light chain lambda amyloid production. *Cancer* 82(2), 362-374.

25   Hammers A, Allom R, Koepp MJ, Free SL, Myers R, Lemieux L, Mitchell TN, Brooks DJ, Duncan JS (2003) Three-dimensional maximum probability atlas of the human brain, with particular reference to the temporal lobe. *Hum Brain Mapp* 19(4), 224-247.

26   Ossenkoppele R, Tolboom N, Foster-Dingley JC, Adriaanse SF, Boellaard R, Yaqub M, Windhorst AD, Barkhof F, Lammertsma AA, Scheltens P, van der Flier

WM, van Berckel BN (2012) Longitudinal imaging of Alzheimer pathology using [11C]PIB, [18F]FDDNP and [18F]FDG PET. *Eur J Nucl Med Mol Imaging* 39(6), 990-1000.

27   Solomon B, Koppel R, Hanan E, Katzav T (1996) Monoclonal antibodies inhibit in vitro fibrillar aggregation of the Alzheimer beta-amyloid peptide. *Proc Natl Acad Sci USA* 93,452–455

28   Mathis CA, Wang Y, Holt DP, Huang GF, Debnath ML, Klunk WE (2003) Synthesis and evaluation of 11C-labeled 6-substituted 2-arylbenzothiazoles as amyloid imaging agents. *J Med Chem* 46(13), 2740-2754.

29   Ikonomovic MD, Abrahamson EE, Isanski BA, Debnath ML, Mathis CA, Dekosky ST, Klunk WE (2006) X-34 labeling of abnormal protein aggregates during the progression of Alzheimer's disease. *Methods Enzymol* 412, 123-144.

30   Villarejo-Galende A, Sarandeses P, Penas-Prado M, Hernández-Laín A, Ramos A, Hernández-Martínez AC, Carro E, Ricoy JR, Hernández-Gallego J (2015) PET-Florbetapir findings in primary cerebral amyloidoma. *J Neurol* 262(4), 1052-1054.

31   Rowe CC, Villemagne VL (2013) Brain Amyloid Imaging. *J Nucl Med Technol* 41(1), 11-18.

32   Antoni G, Lubberink M, Estrada S, Axelsson J, Carlson K, Lindsjö L, Kero T, Långström B, Granstam SO, Rosengren S, Vedin O, Wassberg C, Wikström G, Westermark P, Sörensen J (2013) In vivo visualization of amyloid deposits in the heart with 11C-PIB and PET. *J Nucl Med* 54(2), 213-20.

33   Hellström-Lindahl E, Westermark P, Antoni G, Estrada S (2014) In vitro binding of[³H]PIB to human amyloid deposits of different types. *Amyloid* 21(1), 21-7.
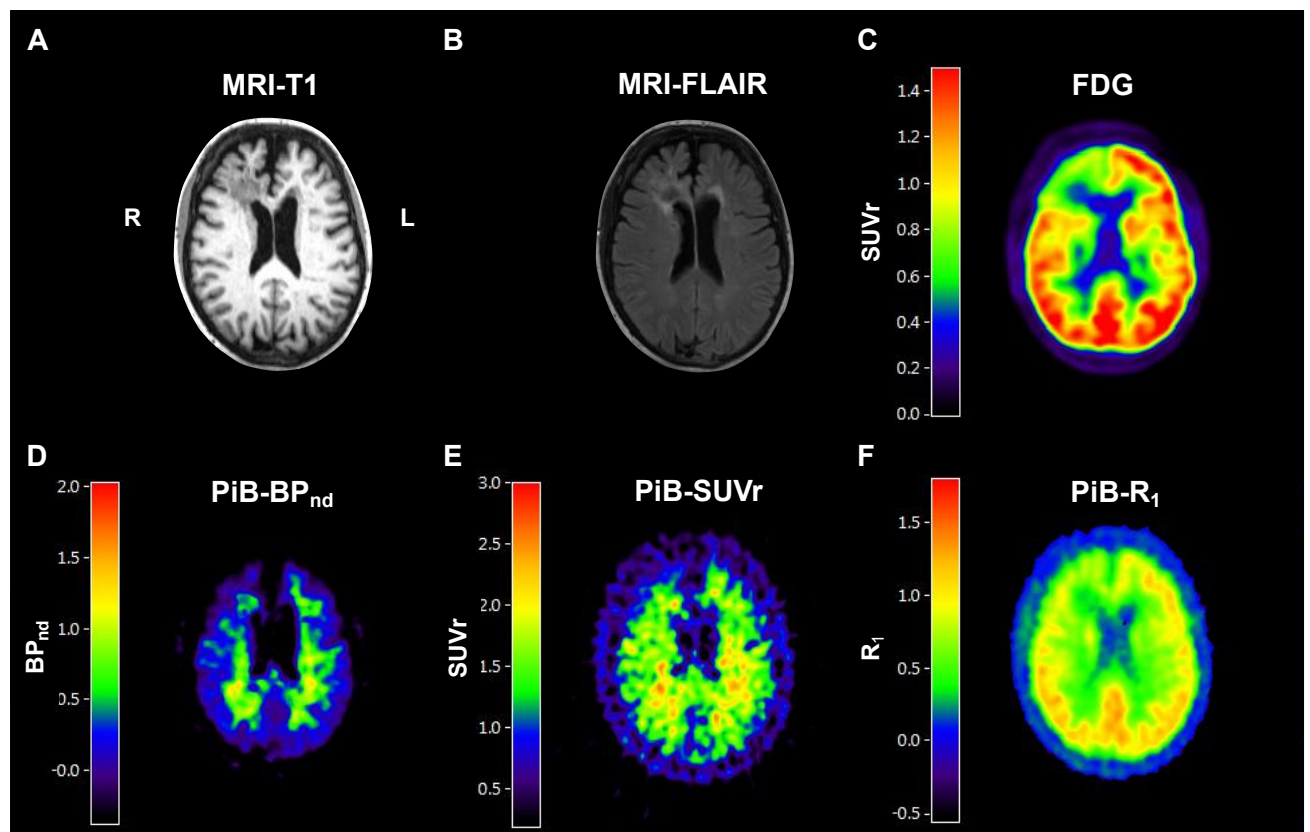
FIGURES

Fig. 1 Axial T1, FLAIR, [18F]FDG-SUVr and [11C]PiB BP_{nd}, SUVr and R_1 PET images of the amyloidoma

T1 (A) and FLAIR (B) images show the intracerebral amyloidoma in the right frontal lobe. FDG-PET (C) shows hypometabolism at the location of the amyloidoma. BP_{nd} (D) and SUVr (E) images reveal lack of PiB-binding in the amyloidoma, while the R_1 (pseudo-flow; F) image indicates that tracer is being delivered to the amyloidoma. FDG – Fluodeoxyglocose, FLAIR – fluid-attenuated inversion recovery, MRI – magnetic resonance imaging, PiB – Pittsburgh compound B, BP_{nd} – non-displaceable binding potential, SUVr – standardized uptake values ratio.
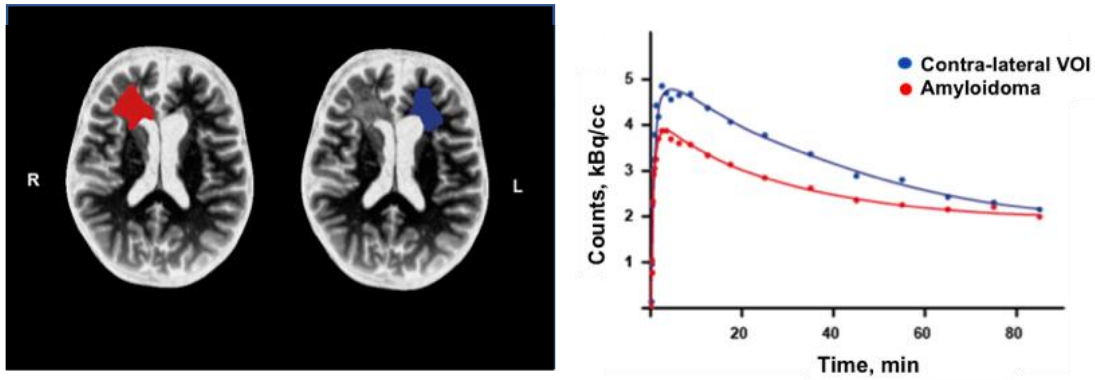
Fig. 2 Amyloidoma and contra-lateral volume of interest

In the left panel, the manual delineation of the amyloidoma is presented in red and the contra-lateral volume-of-interest is presented in blue. The right panel displays time-activity curves of the amyloidoma and contra-lateral volume of interest.

kBq/cc – kilobecquerel per cubic centimeter
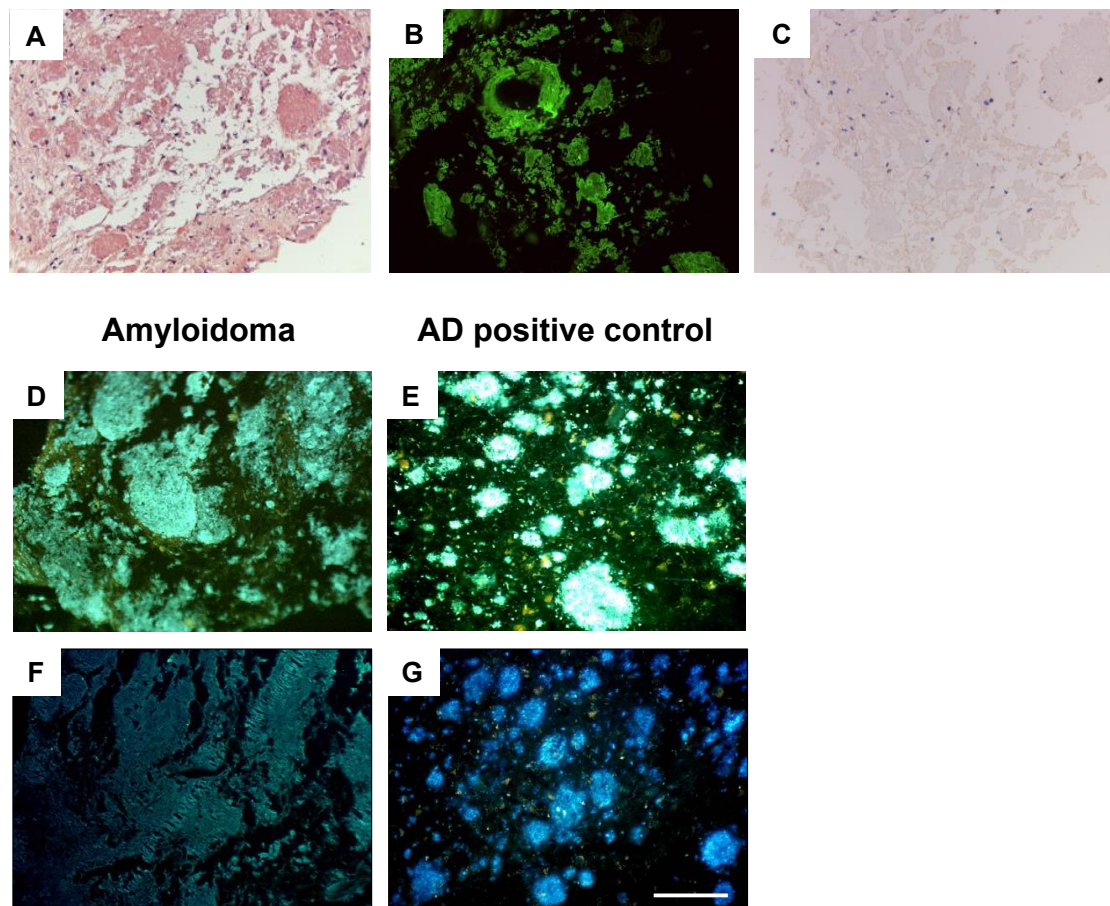
Amyloidoma   **AD positive control**

Fig. 3 Histological staining, immunohistochemistry and histofluorescence in sections from the amyloidoma and additional histofluorescence in frontal cortex of an end-stage AD "positive control"

Congo-red (A) and thioflavin-S (B) stainings indicated presence of amyloid but 6F/3D immunohistochemistry (C) revealed no indication for Aβ pathology. Additional, X-34 histofluorescence in different sections of the biopsy material (D) again revealed presence of amyloid, similar as in the AD positive control (E). However, absence of histofluorescence with 6-CN-PiB in the amyloidoma (F), in contrast to the AD positive control (G), reveals lack of PiB binding.

Scale bar = 75μm